nature nanotechnology

ARTICLES

PUBLISHED ONLINE: 27 JULY 2014 | DOI: 10.1038/NNANO.2014.152

Interconnected hollow carbon nanospheres for stable lithium metal anodes

Guangyuan Zheng[1], Seok Woo Lee[2], Zheng Liang[2], Hyun-Wook Lee[2], Kai Yan[2], Hongbin Yao[2], Haotian Wang[3], Weiyang Li[2], Steven Chu[4] and Yi Cui[2,5]*

For future applications in portable electronics, electric vehicles and grid storage, batteries with higher energy storage density than existing lithium ion batteries need to be developed. Recent efforts in this direction have focused on high-capacity electrode materials such as lithium metal, silicon and tin as anodes, and sulphur and oxygen as cathodes. Lithium metal would be the optimal choice as an anode material, because it has the highest specific capacity (3,860 mAh g^{-1}) and the lowest anode potential of all. However, the lithium anode forms dendritic and mossy metal deposits, leading to serious safety concerns and low Coulombic efficiency during charge/discharge cycles. Although advanced characterization techniques have helped shed light on the lithium growth process, effective strategies to improve lithium metal anode cycling remain elusive. Here, we show that coating the lithium metal anode with a monolayer of interconnected amorphous hollow carbon nanospheres helps isolate the lithium metal depositions and facilitates the formation of a stable solid electrolyte interphase. We show that lithium dendrites do not form up to a practical current density of 1 mA cm^{-2}. The Coulombic efficiency improves to ~99% for more than 150 cycles. This is significantly better than the bare unmodified samples, which usually show rapid Coulombic efficiency decay in fewer than 100 cycles. Our results indicate that nanoscale interfacial engineering could be a promising strategy to tackle the intrinsic problems of lithium metal anodes.

When interest in secondary lithium batteries began to emerge more than four decades ago[1] it was clear that, to make viable Li metal anodes, two fundamental challenges would need to be resolved: (1) accommodating the large change in electrode volume during cycling (unlike graphite and silicon anodes, where lithiation produces volume changes of ~10% and 400%, respectively, Li metal is 'hostless' and its relative volumetric change is virtually infinite); and (2) controlling the reactivity towards the electrolyte (Li is one of the most electropositive elements)[2–6]. Even today, there is still very little control over the thickness, grain size, chemical composition and spatial distribution of the solid electrolyte interphase (SEI), which, together, make the battery inefficient[7,8]. One problem lies in the fact that the SEI layer cannot withstand mechanical deformation and continuously breaks and repairs during cycling. As a result, Li metal batteries have low Coulombic efficiency (80–90% for carbonate solvents and 90–95% for ether solvents)[9] and low cycle life due to the rapid loss of Li and electrolyte in the continuous formation/dissolution of the SEI[10]. A second problem is that Li deposition is not uniform across the electrode surface and can form large dendrites that cause short circuiting of the battery[11–13]. Third, reactions between the Li metal and the electrolytes are exothermic and large surface areas can pose risks of overheating (thermal runaway)[14].

Considerable effort has been directed at addressing these problems using both solid and liquid electrolytes. As solid electrolytes, polymers and ceramics have been developed for their perceived ability to mitigate dendrite nucleation[15,16] and block their growth[17–20]. However, most solid electrolytes have low ionic conductivity, resulting in low power output. Moreover, Li polymer batteries need to be operated at elevated temperatures to achieve reasonable power, at the expense of mechanical stability[20–22]. Ceramic solid electrolytes with a framework structure, such as $Li_{10}GeP_2S_{12}$ and garnet type $Li_7La_3Zr_2O_{12}$, have been investigated for their high Li ion conductivity (~1×10^{-2} to 1×10^{-4} S cm^{-1})[19,23,24], but, like their polymer counterparts, interfacial issues remain largely unresolved[25,26].

In the case of liquid electrolytes, a great deal of research has focused on using additives[27–29] together with chemical passivation of the Li metal surface to reduce electrolyte decomposition[30,31]. However, the thin films formed on the Li metal using these methods consist mainly of Li compounds, which are brittle and have limited cohesion with the metal surface[32]. Consequently, upon Li deposition, the film surface usually cracks as a result of volumetric expansion, exposing fresh Li metal for further reactions (Fig. 1a). Lithium dissolution then takes place, creating pits and crevices with low impedance[33], and Li ions flow at the defects, leading to rapid growth of metal filaments and dendrites. Stabilizing the interface between the Li metal and the electrolyte is therefore key in improving the cycling performance of Li metal batteries.

The ideal interfacial layer for the Li metal anode needs to be chemically stable in a highly reducing environment, and also mechanically strong. High flexibility is desired to accommodate the volumetric expansion of Li deposition without mechanical damage. In addition, the ability to control the flow of Li ions with the SEI inhomogeneities is essential to ensure uniform Li deposition[33]. Here, we describe a flexible, interconnected, hollow amorphous carbon nanosphere coating with the aim of realizing such an ideal interfacial layer (Fig. 1b). The advantages of our approach are threefold: (1) amorphous carbon is chemically stable when in contact with Li metal; (2) the thin amorphous carbon layer does not increase the impedance to charge transfer, but has a Young's modulus[34] of ~200 GPa, high enough to suppress Li dendrite

[1]Department of Chemical Engineering, Stanford University, Stanford, California 94305-5025, USA, [2]Department of Materials Science and Engineering, Stanford, California 94305-4034, USA, [3]Department of Applied Physics, Stanford, California 94305, USA, [4]Department of Physics, Stanford University, Stanford, California 94305, USA, [5]Stanford Institute for Materials and Energy Sciences, SLAC National Accelerator Laboratory, 2575 Sand Hill Road, Menlo Park, California 94025, USA. *e-mail: yicui@stanford.edu

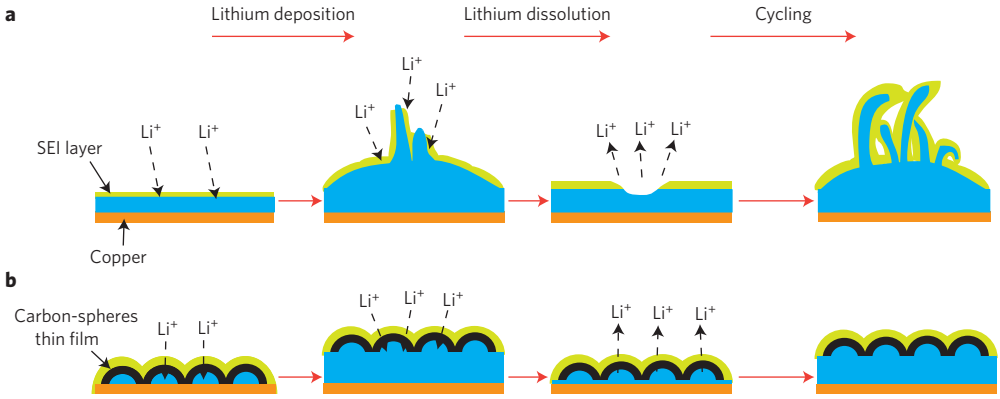

Figure 1 | Schematic diagrams of the different Li anode structures. a, A thin film of SEI layer forms quickly on the surface of deposited Li (blue). Volumetric changes during the Li deposition process can easily break the SEI layer, especially at high current rates. This behaviour leads to ramified growth of Li dendrites and rapid consumption of the electrolytes. **b**, Modifying the Cu substrate with a hollow carbon nanosphere layer creates a scaffold for stabilizing the SEI layer. The volumetric change of the Li deposition process is accommodated by the flexible hollow-carbon-nanosphere coating.

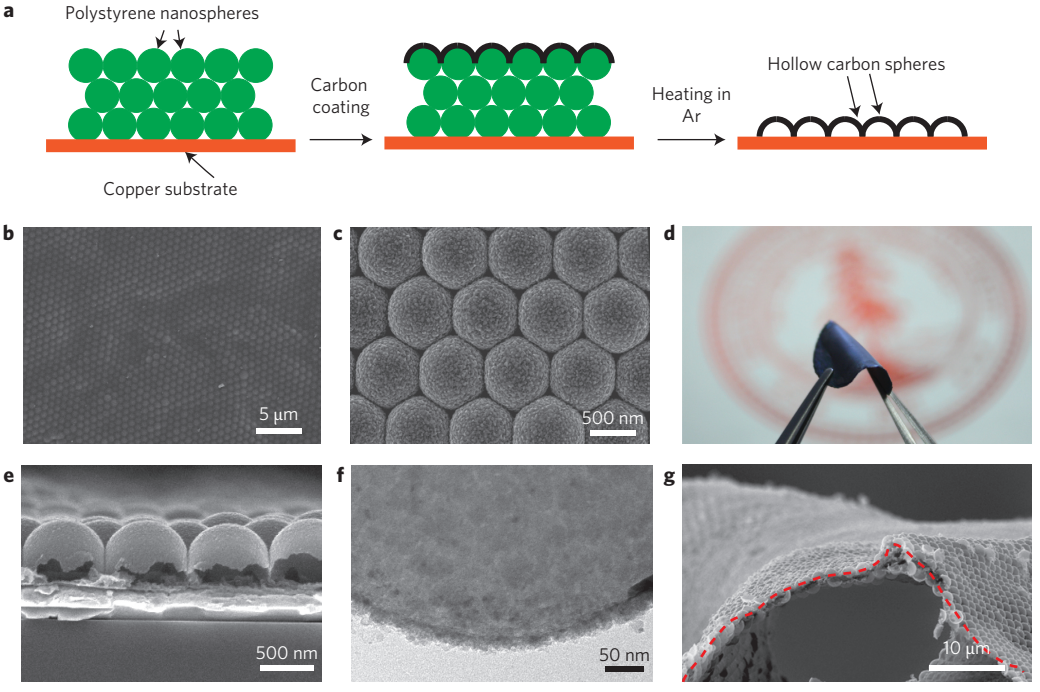

Figure 2 | Fabrication of hollow carbon nanosphere-coated electrode. a, Fabrication process for the hollow carbon nanosphere-modified Cu electrode. Left to right: Polystyrene nanoparticles are first deposited onto the Cu substrate; a thin film of amorphous carbon is coated on top of the polystyrene array using flash-evaporation of carbon cord; thermal decomposition of the polystyrene template results in the formation of interconnected hollow carbon nanospheres. **b**,**c**, SEM images of the carbon-coated polystyrene nanoparticle array at low (**b**) and high (**c**) magnifications. The slight morphology change of the carbon nanospheres to a hexagonal shape could be due to the elevated temperature during the carbon-coating process. **d**, Digital camera image of the as-fabricated hollow carbon nanosphere thin film after removal of the polystyrene template. **e**, Cross-sectional SEM image of the hollow carbon nanospheres. **f**, TEM image of the hollow carbon nanospheres, with wall thickness of ~20 nm. **g**, SEM image of the hollow carbon nanosphere thin-film peeled off the Cu substrate. Red dashed line: trace of the curvature of bending.

growth (theoretical calculations have shown that a solid film with modulus higher than 6 GPa should be sufficient to this end[20]); and (3) a hollow nanosphere layer is weakly bound to the metal current collector and can move up and down to adjust the availability of empty space during cycling. The top surface, formed from the hollow carbon nanospheres, is static and forms a stable, conformal SEI, while Li metal deposition takes place underneath, on the metal current collector. The stable SEI on the carbon nanosphere surface helps reduce the flow of Li ions towards the regions of broken SEI on the metal current collector (Supplementary Fig. 1).

Fabrication of electrode

We have developed a template synthesis method for fabricating the hollow carbon nanopheres, using vertical deposition of polystyrene nanoparticles (Fig. 2a). A colloidal multilayer opal structure is formed on Cu foil by slowly evaporating a 4% aqueous solution of carboxylated polystyrene particles. The highly monodisperse polystyrene nanoparticles form a close-packed thin film with long-range order (Fig. 2b)[35]. The polystyrene nanoparticles are coated with a thin film of amorphous carbon using flash evaporation of carbon fibres (Fig. 2c). The slight morphology change of the

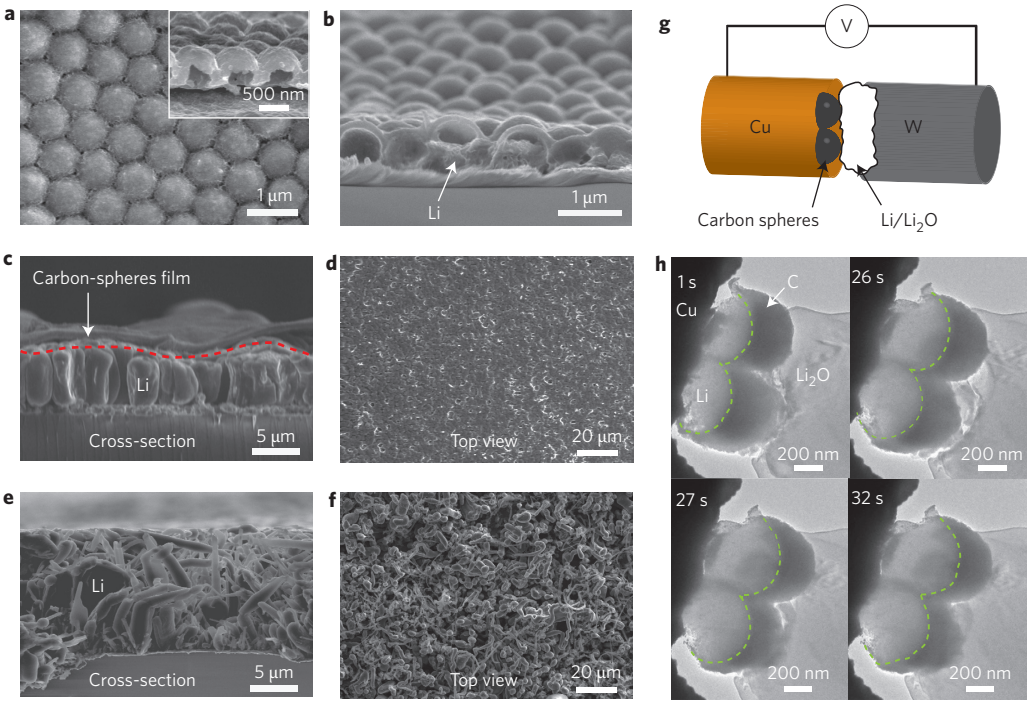

Figure 3 | Li deposition on a Cu substrate with and without carbon nanosphere modification. a, Top-view SEM image of hollow carbon nanospheres after the initial SEI formation process. Inset: the hollow carbon nanosphere structure is preserved after SEI coating. **b**, Cross-sectional SEM image showing the initial deposition of Li metal under carbon nanospheres. **c**, Deposited Li elevates the hollow carbon nanosphere thin film due to weak binding with the Cu substrate. The carbon nanosphere coating allows more uniform Li flux, and the deposited Li is columnar rather than dendritic. **d**, Top-view SEM image showing the smooth surface of the electrode with the carbon nanosphere modification. **e**, For the electrode without carbon nanosphere modification, ramified growth of mossy Li/dendrites is clearly observed. **f**, Corresponding top-view SEM image of the electrode without modification. **g**, Schematic showing the configuration of the *in situ* TEM cell. Hollow carbon nanospheres are grown on a Cu wire, serving as the working electrode. The counter-electrode consists of a small piece of Li metal coated with Li_2O (solid electrolyte) on the tip of a W wire. A voltage bias of about −5 V is applied between the two electrodes to drive Li deposition. **h**, TEM images of the Li deposition process on Cu wires decorated with hollow carbon nanospheres taken at different times. Li metal approaches the carbon nanospheres from the right, and deposition is observed once a voltage bias is applied. See Supplementary Information for full movie.

carbon nanospheres to a hexagonal shape could be due to the elevated temperature during the carbon coating process. The samples are then heated in a tube furnace to 400 °C under an inert atmosphere, forming hollow carbon nanopheres on the Cu substrate (Fig. 2e). Transmission electron microscope (TEM) characterization shows that the carbon wall has a thickness of ~20 nm (Fig. 2f). The hemispherical carbon nanospheres are interconnected to form a thin film (Supplementary Fig. 2a), which can be peeled off the Cu surface easily (Supplementary Fig. 2b). Loose attachment of the carbon film to the Cu electrode is important in that it allows the protective film to be lifted up, creating space for Li deposition. Mechanical flexibility is also important in accommodating the volumetric change of Li deposition and dissipating the stress exerted on the Li protection layer during cycling. A digital camera image (Fig. 2d) and scanning electron microscopy (SEM) image (Fig. 2g) show that the carbon nanosphere thin film can achieve a bending radius of ~20 μm.

SEM characterization of Li deposition

The top surface of evaporated carbon is highly insulating due to the large amount of tetrahedral bondings[36], while the bulk has a conductivity of ~7.5 S m^{-1}, as calculated from four-point-probe measurements (Supplementary Fig. 3). The low conductivity of the evaporated carbon is a result of the lack of long-range order in its structure and can reduce direct Li deposition onto the carbon[37]. The graphitic regions would initially be lithiated and form a stable SEI on top of the carbon nanospheres to prevent penetration of solvent molecules (Supplementary Fig. 4a). Figure 3a presents a top view of the hollow carbon nanospheres after SEI formation. The cross-sectional image in the inset to Fig. 3a shows that the hollow nanosphere structure is preserved after cycling. The electrochemical performance of the as-fabricated anode structure was tested using constant current polarization. Figure 3b shows the hollow-nanosphere-modified electrode at the beginning of Li deposition. Li metal starts to nucleate within the hollow carbon nanospheres on the Cu substrate, and, as Li continues to deposit, granular Li begins to grow, elevating the hollow carbon nanosphere film (Fig. 3c, Supplementary Fig. 4e), confirming our design of depositing Li metal underneath the carbon. The deposited Li metal has a column-like morphology with a diameter of ~3.0 ± 0.3 μm, with no long filaments or dendrites protruding, as is common when Li is deposited on bare Cu (Fig. 3e). The drastic change in morphology is a good indication of the lack of an SEI layer on the deposited Li, allowing the Li to merge. In the control cell, the deposited Li is immediately passivated by the SEI layer, which prevents the Li metal from merging, thus significantly increasing the surface area. As shown in Fig. 3d, after 50 cycles of charge/discharge at 1 mA cm^{-2}, the top surface of the electrode is relatively uniform, without an overgrowth of Li dendrites. In contrast, direct deposition of Li metal onto a Cu electrode results in a very uneven growth of mossy Li, with thin Li filaments clearly visible (Fig. 3f). Another control sample tested involved the cycling of Li on a flat carbon-coated Cu electrode without nanosphere morphology (Supplementary Fig. 6). Similar to a previous study on an amorphous carbon thin-film-coated electrode[38], the rigid carbon coating tends to crack upon cycling, and the Coulombic efficiency drops rapidly after about 50 cycles. Comparison with the flat carbon film therefore highlights the

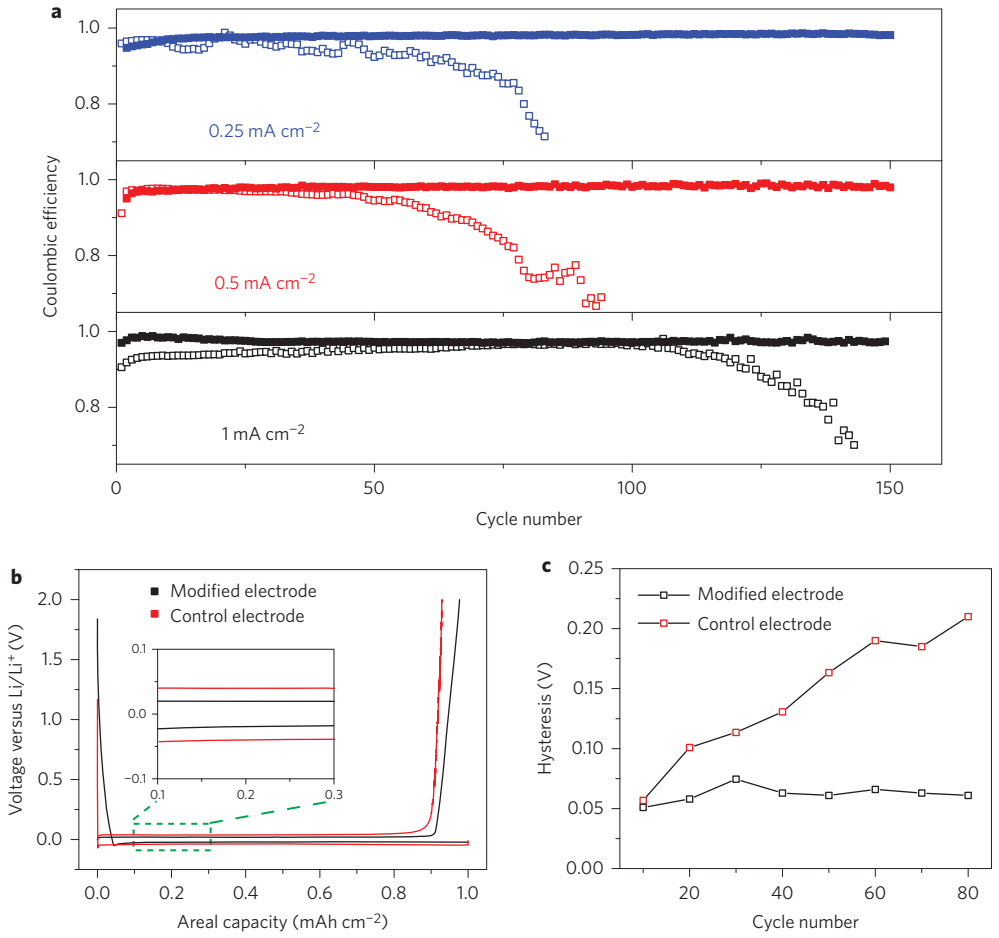

Figure 4 | Electrochemical characterization of the electrodes for Li deposition/dissolution. a, Comparison of cycling performances of the hollow carbon nanosphere-modified electrode (solid symbols) and the control Cu electrode (hollow symbols) at different current rates. The amount of Li deposited in each cycle is 1 mAh cm^{-2}. **b**, Voltage profiles of the Li deposition/dissolution process with Li metal as the reference electrode at 0.5 mA cm^{-2}. **c**, Comparison of the hysteresis of Li deposition/dissolution for the modified electrode and the control electrode with Li metal as the reference/counter-electrode.

differences in the flexibility of the hollow nanosphere interfacial layer and its weak bonding to the Cu current collector.

In situ TEM observation of Li deposition

To further understand the Li deposition phenomenon within the hollow carbon nanospheres, we carried out *in situ* transmission electron microscopy (TEM) experiments[39,40] using a specialized dual-probe biasing TEM holder (Nanofactory Instrument). One probe was a Cu metal wire decorated with hollow carbon nanospheres and the other consisted of a W wire with a small piece of Li metal attached to the tip (Fig. 3g). Because the Li metal was exposed to air for a few seconds when transferring the holder into the TEM, a thin layer of Li_xO formed on the Li metal. This thin oxide layer acts as a solid electrolyte for the nanoscale electrochemical cell. By manipulating a piezoelectric motor on the TEM holder, the hollow carbon nanospheres came into contact with the lithium oxide and a voltage bias was applied to drive the Li ion through the oxide solid electrolyte towards the carbon nanospheres. Figure 3h presents a series of bright-field TEM images of the carbon nanospheres during the Li deposition process. The experiments show that Li begins to deposit on the Cu wire underneath the carbon nanospheres immediately after application of the voltage bias. After about 25 s of Li deposition, the average thickness of the Li increased by 26%. Further deposition for another 6 s increased the Li thickness by another 25%. The morphology change of the deposited Li in lifting up the carbon nanospheres can be seen in the Supplementary Movie, which confirms, visually, the concept of depositing Li underneath carbon while maintaining the integrity of the carbon nanospheres.

Electrochemical testing of the modified electrodes

The demonstrated stable interfacial layer of carbon hollow nanospheres opens up the opportunity to improve the Coulombic efficiency of Li metal anodes. Coulombic efficiency is an important parameter for long cycle life and is defined as the ratio of the amount of Li that is stripped from the working electrode versus the amount that is plated during each cycle. Because the cycle life of batteries with Li metal electrodes is related to electrolyte decomposition[23,24], a fair comparison of electrode performance is to use a controlled amount of electrolytes. To standardize the electrochemical performance, ~30 µl electrolytes was used in each coin cell test. In the half-cell configuration Li was electrochemically deposited (at 1 mAh cm^{-2}) from the Li metal counter-electrode onto the hollow nanosphere-modified working electrode and then stripped away. Here, the Coulombic efficiency reflects the loss on the working electrode, because the Li metal counter-electrode has excess Li. In cycle life testing these batteries fail due to the depletion of electrolytes as a result of reaction with the Li metal[8]. Consequently, the internal resistance increases rapidly in batteries that have severe electrolyte decomposition. The reduced electrolyte contact with active material also results in a pronounced increase in local current density, which subsequently leads to more dendrite formation[41]. The analysis of electrochemical performance shows that the cycling performance of the Li metal working electrodes

with the carbon nanosphere coating is significantly improved. The Coulombic efficiency is maintained at ~99% for more than 150 cycles at 0.25 mA cm^{-2} and ~98.5% at 0.5 mA cm^{-2} (Fig. 4a). In comparison, cells without the hollow carbon nanosphere coating show a gradual decrease in Coulombic efficiency, which eventually drops to less than 50% after 100 cycles at 0.25 mA cm^{-2} and 0.5 mA cm^{-2}. In the control sample with Cu foil coated with flat carbon film only, the performance is also relatively poor, with the Coulombic efficiency dropping to below 90% after 70 cycles (Supplementary Fig. 6). When tested at a high current density of 1 mA cm^{-2}, the Coulombic efficiency of the Li metal working electrode with a carbon nanosphere coating is maintained at ~97.5% for more than 150 cycles, while the control Cu electrode showed rapid decay after 100 cycles. Using an alternative testing method proposed by Aurbach and co-workers (Supplementary Methods)[42], in which 2.5 mA cm^{-2} of Li was initially deposited, followed by 10 cycles of deposition/dissolution of 0.5 mAh cm^{-2} Li, we were able to achieve a Coulombic efficiency of ~99.5% at 0.5 mA cm^{-2}, which is higher than the previous results. For example, Li metal cycling in ether-based electrolyte usually has a Coulombic efficiency of ~95–98% (refs 8,43). There have also been attempts to use electrolyte additives[28–30] and other conditions, such as the application of high pressure[33], to improve Li metal performance. Those results usually show low Coulombic efficiency but with large variation during cycling (sometimes reaching more than 100% for a few cycles)[44]. The sporadic high Coulombic efficiency is probably due to the activation of disconnected mossy Li from previous cycles. However, the Li metal batteries in the present study show consistently stable, high-Coulombic-efficiency cycling, which can be attributed to the more uniform Li deposition under the hollow carbon nanospheres, more stable SEI formation on top of the spheres, and reduction of electrolyte decomposition.

Impedance spectroscopy revealed that the carbon-nanosphere-modified electrode has lower interfacial charge transfer resistance than the control electrode due to the preservation of a stable SEI layer (Supplementary Fig. 4). The effect of stable SEI formation and reduction of electrolyte decomposition can also be seen in the reduction of polarization (hysteresis) in the voltage profile during Li deposition/dissolution. The Li deposition voltage for the modified electrode is approximately –25 mV (versus Li/Li^+), whereas that for the pristine Cu is ~50 mV. The Li dissolution is 25 mV and 50 mV, respectively (Fig. 4b). For the electrode without modification, the voltage hysteresis in the Li deposition/dissolution increases gradually as the cycle number increases, with a difference in potential of ~210 mV after 80 cycles (Fig. 4c). With the hollow carbon nanosphere modification, the hysteresis is much smaller, only ~50 mV after 50 cycles. This smaller hysteresis is attributed to the lower charge transfer and internal resistance resulting from the thinner SEI layer, which are also evident in the cycling of the different anodes with $LiFePO_4$ cathodes (Supplementary Fig. 5b). The hollow-carbon-nanosphere thin film can be transferred onto the Li metal foil to be paired with Li-containing cathode materials such as $LiFePO_4$ for high-energy-density batteries (Supplementary Fig. 5a).

Conclusions

We have shown that an interfacial layer of hollow carbon nanospheres allows stable Li metal anode cycling up to a practical current density of 1 mA cm^{-2} and with an areal capacity of 1 mAh cm^{-2}. The cycling Coulombic efficiency can be highly stable at ~99% for more than 150 cycles. Future research is needed to develop the application of this approach to practical batteries (the Coulombic efficiency needs to be improved to >99.9% for practical batteries, and alternative electrolyte combinations need to be developed to meet different battery chemistries). A viable route to this end could be to combine the nanoscale engineering approach described here with electrolyte additives. Anodes with interfacial layers on the current collector could be combined with cathodes with preloaded Li ions, such as the existing Li metal oxides and Li_2S. Our work demonstrates that the interfacial nanoscale engineering approach can improve Li metal cycling performance. We believe that the nanoengineering concepts we have described may be a viable route towards Li metal anode batteries and, more specifically, to high-energy-density batteries, such as Li–S and Li–O_2.

Methods

Fabrication of modified electrode. A 100 µl volume of polystyrene nanoparticles (0.78 µm) aqueous suspension (4 wt/wt%, Thermal Scientific) was dropcast onto a Cu foil disk (7/16 inch) and the solvent allowed to evaporate at room temperature for ~2 h. The polystyrene nanoparticles then self-assembled into a hexagonally close-packed structure. The vertical deposition of colloidal crystal was a result of the small density difference between the polystyrene nanoparticles and the solvents. As a result, the evaporation velocity of the colloidal solvent exceeded the sedimentation velocity of the nanoparticles, allowing the nanoparticles to accumulate at the solvent–air interface. As particle concentration increased, lateral capillary immersion forces arranged the nanoparticles into hexagonal packing[45]. To form carbon nanospheres, the close-packed polystyrene nanoparticles were first coated with amorphous carbon in a carbon coater (EMS150R ES). Carbon fibres were used as the evaporation target. The evaporation chamber was pumped down to 5×10^{-2} mbar before an outgassing current of 30 A was passed through the carbon fibres. After outgas recovery, a pulse current was passed through the fibre to allow flash-evaporation of carbon. The pulse current was set to 60 A for 20 s, with a 10 s interval between pulses. To remove the polystyrene templates, the sample was placed in a tube furnace and heated under Ar at 400 °C for 1.5 h (ramping rate of 5 °C min^{-1}). The hollow carbon nanospheres were plasma-treated to facilitate the formation of a stable SEI (Supplementary Fig. 2c), and the electrode was then coated with polyvinyldene fluoride (PVDF) by spin-coating 100 µl of 5% PVDF solution in *N*-methyl pyrrolidone (NMP) onto the sample (1,000 r.p.m. for 1 min). NMP solvent was removed by placing the samples in a vacuum oven for 3 h at 50 °C. To transfer the hollow-carbon-nanosphere thin film onto the Li metal anode, the Cu substrate used in the fabrication process was etched away in $(NH_4)_2S_2O_8$ solution and the thin film dried in a vacuum oven before being pressed onto the Li metal anode.

Fabrication of the control electrode. The control electrode was fabricated by first spin-coating a thin layer of PVDF onto the Cu current collector. After drying, the electrode was assembled in a coin cell with Li metal as both the reference and counter-electrode. Pretreatment of the control electrode was carried out as in the modified electrode by cycling the battery between 0 and 2 V for 10 cycles. The electrode was then tested by depositing and dissolving a controlled amount of Li at different current densities.

Electrochemical testing. Galvanostatic experiments were performed using a 96-channel battery tester (Arbin Instrument). The working electrodes were assembled in 2032-type coin cells (MTI Corporation) with Li metal (Alfa Aesar) as the reference electrode and counter-electrode. The electrolyte was 1 M lithium bis (trifluoromethanesulphonyl)imide (LiTFSI) in 1,3-dioxolane and 1,2-dimethoxyethane (volume ratio 1:1) with 1% lithium nitrate ($LiNO_3$) and 100 mM Li_2S_8 additives. The presence of $LiNO_3$ and Li_2S_8 helps in the formation of a stable SEI on the Li metal electrode. For the coloumbic efficiency test, Li metal was used as both the working and reference electrodes. The Li metal reference electrode was soaked in a 2% $LiNO_3$ solution in DOL/DME overnight before assembling the coin cells. To standardize the testing, 30 µl electrolytes was used in each coin cell testing. The batteries were first cycled between 0 V and 2 V to form a stable SEI on the hollow carbon spheres (Supplementary Fig. 2d). Cycling tests were carried out by first depositing 1 mAh of Li onto the Cu electrode, followed by Li stripping up to 2 V. To test the modified anode in a full cell, $LiFePO_4$ (MTI Corp) at 1 mAh cm^{-2} was used as the cathode material. Measurements of a.c. impedance were carried out using a Bio-Logic VMP3 tester with a frequency range between 0.1 Hz and 1 MHz.

Received 17 February 2014; accepted 26 June 2014; published online 27 July 2014

References

1. Whittingham, M. S. Electrical energy storage and intercalation chemistry. *Science* **192,** 1126–1127 (1976).
2. Ohzuku, T., Iwakoshi, Y. & Sawai, K. Formation of lithium–graphite intercalation compounds in nonaqueous electrolytes and their application as a negative electrode for a lithium ion (shuttlecock) cell. *J. Electrochem. Soc.* **140,** 2490–2498 (1993).
3. Chan, C. K. *et al.* High-performance lithium battery anodes using silicon nanowires. *Nature Nanotech.* **3,** 31–35 (2008).
4. Tarascon, J. M. & Armand, M. Issues and challenges facing rechargeable lithium batteries. *Nature* **414,** 359–367 (2001).

5. Armand, M. & Tarascon, J. M. Building better batteries. *Nature* **451,** 652–657 (2008).
6. Bruce, P. G., Freunberger, S. A., Hardwick, L. J. & Tarascon, J. M. Li–O_2 and Li–S batteries with high energy storage. *Nature Mater.* **11,** 19–29 (2012).
7. Peled, E. The electrochemical behavior of alkali and alkaline earth metals in nonaqueous battery systems—the solid electrolyte interphase model. *J. Electrochem. Soc.* **126,** 2047–2051 (1979).
8. Aurbach, D. *et al.* Attempts to improve the behavior of Li electrodes in rechargeable lithium batteries *J. Electrochem. Soc.* **150,** L6 (2003).
9. Ota, H. *et al.* Characterization of lithium electrode in lithium imides/ethylene carbonate and cyclic ether electrolytes: II. Surface chemistry. *J. Electrochem. Soc.* **151,** A437–A446 (2004).
10. Xu, K. Nonaqueous liquid electrolytes for lithium-based rechargeable batteries. *Chem. Rev.* **104,** 4303–4418 (2004).
11. Bhattacharyya, R. *et al. In situ* NMR observation of the formation of metallic lithium microstructures in lithium batteries. *Nature Mater.* **9,** 504–510 (2010).
12. Chandrashekar, S. *et al.* ^{7}Li MRI of Li batteries reveals location of microstructural lithium. *Nature Mater.* **11,** 311–315 (2012).
13. Harry, K. J. *et al.* Detection of subsurface structures underneath dendrites formed on cycled lithium metal electrodes. *Nature Mater.* **13,** 69–73 (2013).
14. Von Sacken, U., Nodwell, E., Sundher, A. & Dahn, J. R. Comparative thermal stability of carbon intercalation anodes and lithium metal anodes for rechargeable lithium batteries. *J. Power Sources* **54,** 240–245 (1995).
15. Chazalviel, J. N. Electrochemical aspects of the generation of ramified metallic electrodeposits. *Phys. Rev. A* **42,** 7355–7367 (1990).
16. Rosso, M. *et al.* Onset of dendritic growth in lithium/polymer cells. *J. Power Sources* **97-98,** 804–806 (2001).
17. Yu, X., Bates, J. B., Jellison, G. E. & Hart, F. X. A stable thin-film lithium electrolyte: lithium phosphorus oxynitride. *J. Electrochem. Soc.* **144,** 524–532 (1997).
18. Nimon, Y. S., Chu, M-Y. & Visco, S. J. Coated lithium electrodes. US patent US6537701 B1 (2003).
19. Kamaya, N. *et al.* A lithium superionic conductor. *Nature Mater.* **10,** 682–686 (2011).
20. Stone, G. M. *et al.* Resolution of the modulus versus adhesion dilemma in solid polymer electrolytes for rechargeable lithium metal batteries. *J. Electrochem. Soc.* **159,** A222–A227 (2012).
21. Croce, F., Persi, L., Ronci, F. & Scrosati, B. Nanocomposite polymer electrolytes and their impact on the lithium battery technology. *Solid State Ionics* **135,** 47–52 (2000).
22. Zaghib, K. Lithium metal vs. Li-ion batteries: challenges and opportunities. *ECS Meeting Abstracts* **MA2013-02,** 952 (2013).
23. Murugan, R., Thangadurai, V. & Weppner, W. Fast lithium ion conduction in garnet-type $Li_7La_3Zr_2O_{12}$. *Angew. Chem. Int. Ed.* **46,** 7778–7781 (2007).
24. Thangadurai, V., Narayanan, S. & Pinzaru, D. Garnet-type solid-state fast Li ion conductors for Li batteries: critical review. *Chem. Soc. Rev.* **43,** 4714–4727 (2014).
25. Xu, W. *et al.* Lithium metal anodes for rechargeable batteries. *Energy Environ. Sci.* **7,** 513–537 (2014).
26. Kim, K. H. *et al.* Characterization of the interface between $LiCoO_2$ and $Li_7La_3Zr_2O_{12}$ in an all-solid-state rechargeable lithium battery. *J. Power Sources* **196,** 764–767 (2011).
27. Crowther, O. & West, A. C. Effect of electrolyte composition on lithium dendrite growth. *J. Electrochem. Soc.* **155,** A806–A811 (2008).
28. Hirai, T., Yoshimatsu, I. & Yamaki, J-I. Effect of additives on lithium cycling efficiency. *J. Electrochem. Soc.* **141,** 2300–2305 (1994).
29. Ding, F. *et al.* Dendrite-free lithium deposition via self-healing electrostatic shield mechanism. *J. Am. Chem. Soc.* **135,** 4450–4456 (2013).
30. Marchioni, F. *et al.* Protection of lithium metal surfaces using chlorosilanes. *Langmuir* **23,** 11597–11602 (2007).
31. Ishikawa, M., Kawasaki, H., Yoshimoto, N. & Morita, M. Pretreatment of Li metal anode with electrolyte additive for enhancing Li cycleability. *J. Power Sources* **146,** 199–203 (2005).
32. Aurbach, D., Zinigrad, E., Cohen, Y. & Teller, H. A short review of failure mechanisms of lithium metal and lithiated graphite anodes in liquid electrolyte solutions. *Solid State Ionics* **148,** 405–416 (2002).
33. Gireaud, L. *et al.* Lithium metal stripping/plating mechanisms studies: a metallurgical approach. *Electrochem. Commun.* **8,** 1639–1649 (2006).
34. Suk, J. W., Murali, S., An, J. & Ruoff, R. S. Mechanical measurements of ultra-thin amorphous carbon membranes using scanning atomic force microscopy. *Carbon* **50,** 2220–2225 (2012).
35. Xia, Y., Gates, B., Yin, Y. & Lu, Y. Monodispersed colloidal spheres: old materials with new applications. *Adv. Mater.* **12,** 693–713 (2000).
36. Larson, D. M., Downing, K. H. & Glaeser, R. M. The surface of evaporated carbon films is an insulating, high-bandgap material. *J. Struct. Biol.* **174,** 420–423 (2011).
37. Blue, M. D. & Danielson, G. C. Electrical properties of arc-evaporated carbon films. *J. Appl. Phys.* **28,** 583–586 (1957).
38. Arie, A. A. & Lee, J. K. Electrochemical characteristics of lithium metal anodes with diamond like carbon film coating layer. *Diamond Relat. Mater.* **20,** 403–408 (2011).
39. Huang, J. Y. *et al. In situ* observation of the electrochemical lithiation of a single SnO_2 nanowire electrode. *Science* **330,** 1515–1520 (2010).
40. McDowell, M. T. *et al. In situ* TEM of two-phase lithiation of amorphous silicon nanospheres. *Nano Lett.* **13,** 758–764 (2013).
41. Aurbach, D., Zinigrad, E., Teller, H. & Dan, P. Factors which limit the cycle life of rechargeable lithium (metal) batteries. *J. Electrochem. Soc.* **147,** 1274–1279 (2000).
42. Aurbach, D., Gofer, Y. & Langzam, J. The correlation between surface chemistry, surface morphology, and cycling efficiency of lithium electrodes in a few polar aprotic systems. *J. Electrochem. Soc.* **136,** 3198–3205 (1989).
43. Gofer, Y., Ben-Zion, M. & Aurbach, D. Solutions of $LiAsF_6$ in 1,3-dioxolane for secondary lithium batteries. *J. Power Sources* **39,** 163–178 (1992).
44. Koch, V. R., Goldman, J. L., Mattos, C. J. & Mulvaney, M. Specular lithium deposits from lithium hexafluoroarsenate/diethyl ether electrolytes. *J. Electrochem. Soc.* **129,** 1–4 (1982).
45. Shimmin, R. G., DiMauro, A. J. & Braun, P. V. Slow vertical deposition of colloidal crystals: a Langmuir–Blodgett process? *Langmuir* **22,** 6507–6513 (2006).

Acknowledgements

G.Z. acknowledges financial support from Agency for Science, Technology and Research (A*STAR), Singapore. The authors thank A. Jaffe for help with the Fourier transform infrared measurement and H. Yuan for help with the conductivity measurements. H.L. was supported by the Basic Science Research Program through the National Research Foundation of Korea (contract no. NRF-2012R1A6A3A03038593).

Author contributions

G.Z and Y.C. conceived and designed the experiments. G.Z performed the experiments. S.W.L. performed the numerical simulation and provided data analysis. H.W.L. conducted *in situ* TEM characterization. G.Z. and Y.C. co-wrote the paper. All authors discussed the results and commented on the manuscript.

Additional information

Supplementary information is available in the online version of the paper. Reprints and permissions information is available online at www.nature.com/reprints. Correspondence and requests for materials should be addressed to Y.C.

Competing financial interests

The authors declare no competing financial interests.